*Manuscript
Click here to download Manuscript: Koseoglu et al_OG_2018_MainText_revised.docx Click here to view linked References
: " Disclaimer: This is a pre-publication version. Readers are recommended to consult the full published version for accuracy and citation."

# An assessment of biomarker-based multivariate classification methods versus the $PIP_{25}$ index for paleo Arctic sea ice reconstruction

Denizcan Köseoğlu[a], Simon T Belt[a]*, Katrine Husum[b], Jochen Knies[c,d]

[a] Biogeochemistry Research Centre, School of Geography, Earth and Environmental Sciences, Plymouth University, Plymouth, PL4 8AA, UK.

[b] Norwegian Polar Institute, Fram Centre, NO-9296 Tromsø, Norway.

[c] CAGE – Centre for Arctic Gas Hydrate, Environment and Climate, Department of Geosciences, UiT The Arctic University of Norway, 9037 Tromsø, Norway.

[d] Geological Survey of Norway, N-7491 Trondheim, Norway.

*Author for correspondence

E-mail: sbelt@plymouth.ac.uk

Keywords: Arctic; Sea ice; HBI; Biomarker; Classification Tree; $IP_{25}$; $PIP_{25}$; Barents Sea

: “ Disclaimer: This is a pre-publication version. Readers are recommended to consult the full published version for accuracy and citation.”


## Abstract

The development of various combinative methods for Arctic sea ice reconstruction using the sympagic highly-branched isoprenoid (HBI) $IP_{25}$ in conjunction with pelagic biomarkers has often facilitated more detailed descriptions of sea ice conditions than using $IP_{25}$ alone. Here, we investigated the application of the Phytoplankton-$IP_{25}$ index ($PIP_{25}$) and a recently proposed Classification Tree (CT) model for describing temporal shifts in sea ice conditions to assess the consistency of both methods. Based on biomarker data from three downcore records from the Barents Sea spanning millennial timescales, we showcase apparent and potential limitations of both approaches, and provide recommendations for their identification or prevention. Both methods provided generally consistent outcomes and, within the studied cores, captured abrupt shifts in sea ice regimes, such as those evident during the Younger Dryas, as well as more gradual trends in sea ice conditions during the Holocene. The most significant discrepancies occurred during periods of highly unstable climate change, such as those characteristic of the Younger Dryas–Holocene transition. Such intervals of increased discrepancy were identifiable by significant changes of HBI distributions and correlations to values not observed in proximal surface sediments. We suggest that periods of highly-fluctuating climate that are not represented in modern settings may hinder the performance and complementary application of $PIP_{25}$ and CT-based methods, and that data visualisation techniques should be employed to identify such occurrences in downcore records. Additionally, due to the reliance of both methods on biomarker distributions, we emphasise the importance of accurate and consistent biomarker quantification.

: “ Disclaimer: This is a pre-publication version. Readers are recommended to consult the full published version for accuracy and citation.”

## 1. Introduction

Arctic sea ice is a pivotal component of the global ecosystem. The receding sea ice edge is a site of primary productivity during the spring-summer melt season (e.g., Wassmann et al., 2006; Vancoppenolle et al., 2013, and references therein), while ice formation facilitates deep water formation and helps to maintain the global thermohaline circulation (e.g., Bitz et al., 2006). Additionally, sea ice is an effective reflector of incoming shortwave solar radiation, thus regulating the oceanic heat budget (e.g., Meier et al., 2014, and references therein) and the ocean-atmosphere heat exchange (Maykut, 1978). The sensitivity of the melting-freezing cycle and physical properties of sea ice to the global atmospheric and oceanic circulation of moisture and heat (e.g., Smedsrud et al., 2013) makes seasonal and interannual variability of sea ice cover a prime indicator of climate change (Vihma, 2014). The decline of Arctic sea ice extent and thickness observed via satellite passive microwave sensors since the 1970’s (Lindsay and Schweiger, 2015; Fetterer et al., 2017) is unprecedented within observational records covering recent centuries, at least (Divine and Dick, 2006; Walsh et al., 2017). Cumulative thinning and retreat of Arctic sea ice leads to pre-disposition of the ice cover for accelerated melting via various positive feedback mechanisms (Perovich and Polashenski, 2012), and augments the global temperature increase at high latitudes (Serreze and Barry, 2011). Thus, the Arctic is projected to become ice-free at its September minimum within the next few decades (Overland and Wang, 2013) due to potentially irreversible loss of ice cover (e.g., Lindsay and Zhang, 2005; Eisenman and Wettlaufer, 2009), with important implications for global oceanographic regimes, atmospheric heat circulation (Smedsrud et al., 2013), mid-latitude weather (Mori et al., 2014), Arctic food webs (Harada, 2016), and human activities (Meier et al., 2014). The assessment of such implications and accurate prediction of future trends requires the reconstruction of sea ice cover over geologically significant timescales (Stroeve et al., 2015).

: " Disclaimer: This is a pre-publication version. Readers are recommended to consult the full published version for accuracy and citation."

$IP_{25}$, a source-specific highly-branched isoprenoid (HBI) biomarker synthesized by sympagic diatoms (Brown et al., 2014), has emerged as a relatively direct proxy of seasonal Arctic sea ice (Belt et al., 2007; Belt and Müller, 2013), Consistent with its source, $IP_{25}$ has been detected throughout the Arctic in surface sediments characterised by seasonal sea ice cover (Belt et al., 2007, 2015; Navarro-Rodriguez et al., 2013; Stoynova et al., 2013; Weckström et al., 2013; Xiao et al., 2013, 2015a; Ribeiro et al., 2017), and is mostly absent in ice-free settings (Müller et al., 2012; Méheust et al., 2013). Additionally, $IP_{25}$ appears to be relatively stable within sedimentary records for millions of years (Stein and Fahl, 2013; Knies et al., 2014; Stein et al., 2016). Combined, the seasonal sea ice selectivity, source-specificity and stability have facilitated the use of $IP_{25}$ for palaeo-sea ice reconstructions throughout the Arctic spanning a range of timescales (e.g., Andrews et al., 2009; Müller et al., 2009, 2012; Vare et al., 2010; Stein and Fahl, 2012, 2013; Berben et al., 2014, 2017; Knies et al., 2014, 2017; Müller and Stein, 2014; Belt et al., 2015; Xiao et al., 2015b; Cabedo-Sanz and Belt, 2016; Cabedo-Sanz et al., 2016; Hoff et al., 2016; Stein et al., 2016; Bartels et al., 2017). However, while relative changes in $IP_{25}$ concentration are generally consistent with corresponding shifts in sea ice conditions (Massé et al., 2008; Andrews et al., 2009; Vare et al., 2010; Axford et al., 2011), the considerable differences between absolute sedimentary $IP_{25}$ concentration ranges for locations experiencing similar sea ice conditions (Stoynova et al., 2013; Xiao et al., 2015b) limits comparison of sea ice variability for different Arctic regions.

To help provide more detailed and regionally comparable descriptions of sea ice conditions, Müller et al. (2011) first introduced the Phytoplankton-$IP_{25}$ index ($PIP_{25}$; Eq. 1), based on $IP_{25}$ abundance relative to that of open-water biomarkers produced by marine phytoplankton, such as brassicasterol and dinosterol (Volkman, 1986, 2006). Thus, a normalised uniform scale (0–1) removed the influence of absolute concentrations, allowing

: " Disclaimer: This is a pre-publication version. Readers are recommended to consult the full published version for accuracy and citation."

more consistent comparisons of sea ice conditions between Arctic regions, while a concentration balance factor (i.e. *c*-factor) compensated for different concentration ranges commonly observed for $IP_{25}$ and sterols (Müller et al., 2011; Cabedo-Sanz and Belt, 2016). In practice, correlation of sterol-based $PIP_{25}$ indices and overlying sea ice concentrations yielded variable results for different Arctic regions (Müller et al., 2011; Navarro-Rodriguez et al., 2013; Xiao et al., 2015b), partially attributed to the lower source specificity of sterols, which are produced ubiquitously by a variety of marine, terrigenous (Yunker et al., 2005; Rampen et al., 2010), and even ice-obligate sources (Belt et al., 2013, 2018). Moreover, the value of the *c*-factor greatly affected $PIP_{25}$ estimates in downcore records due to large and variable differences in $IP_{25}$ and sterol concentration ranges in different core sections representing periods of abrupt shifts between contrasting climate conditions (Belt and Müller, 2013; Berben et al., 2014; Cabedo-Sanz and Belt, 2016). More recently, substitution of sterols with a source-specific tri-unsaturated HBI biomarker (hereafter referred to as HBI III (Z); Fig. 1) derived from some pelagic *Pleurosigma* and *Rhizosolenia* spp. (Belt et al., 2000, 2017; Rowland et al., 2001) has significantly reduced the influence of the *c*-factor, in some cases (e.g., Belt et al., 2015; Cabedo-Sanz and Belt, 2016), as a result of comparable concentration ranges of $IP_{25}$ and HBI III (Z). A regional calibration of $P_{III}IP_{25}$ (i.e. $PIP_{25}$ using HBI III (Z) as the pelagic biomarker) versus satellite-derived spring sea ice concentration (%SpSIC) allowed calculation of semi-quantitative SpSIC estimates in the Barents Sea and the western Svalbard margin (Eq. 2; Cabedo-Sanz and Belt, 2016; Smik et al., 2016; Berben et al., 2017). Nonetheless, the magnitude of the *c*-factor, which relies on average biomarker concentrations throughout a dataset when a regional $P_{III}IP_{25}$–SpSIC calibration is not available (Müller et al., 2011), could still potentially introduce bias to $P_{III}IP_{25}$-derived SpSIC estimates. Further, the objective choice of a suitable pelagic counterpart to the sympagic $IP_{25}$ remains a challenge, and is made more difficult by the inherent limitation of the $PIP_{25}$ index to one such

: " Disclaimer: This is a pre-publication version. Readers are recommended to consult the full published version for accuracy and citation."

biomarker. To address these challenges, Köseoğlu et al. (2018) recently constructed a multivariate classification tree (CT) model (Breiman et al., 1984) using percentage abundances of a group of HBI biomarkers (Fig. 1) in surface sediments encompassing the full range of sea ice variability in the Barents Sea. Each surface sediment was classified into marginal (<10 % satellite SpSIC), intermediate (10–50 % SpSIC) or extensive (>50 % SpSIC) class of sea ice conditions (Fig. 2). The CT model was subsequently used to reconstruct classes of sea ice conditions throughout recent centuries in four short sediment cores collected from Barents Sea sites experiencing variable modern sea ice cover (Vare et al., 2010). For these cores, the CT class predictions were consistent with $P_{III}IP_{25}$-derived semi-quantitative SpSIC estimates and, perhaps more importantly, the observational record of sea ice cover (Divine and Dick, 2006; Walsh et al., 2017). The CT method offered automatic selection of HBI biomarkers that achieved the highest classification rate, quantitative model evaluation via performance metrics, and independence from the *c*-factor. Thus, the CT model was ca. 92 ± 6 % accurate using $IP_{25}$ and a further tri-unsaturated HBI (hereafter HBI III (E); Fig. 1) as primary descriptive variables representing ice algal and pelagic productivity, respectively. HBIs II and III (Z) were utilised as surrogate variables, probably due to their high correlation to $IP_{25}$ and HBI III (E), respectively.

Despite this development, CT models require further evaluation before their wider applicability as a statistical tool for classification of sea ice conditions can be established. Specifically, the agreement of model-derived categorical assessment of sea ice conditions and $PIP_{25}$-derived semi-quantitative SpSIC estimates in sediment cores needs to be determined across longer timescales encompassing major changes in sea ice dynamics, such as those occurring during the Younger Dryas–Holocene transition (e.g., Ślubowska et al., 2005; Rasmussen et al., 2007; Cabedo-Sanz et al., 2013; Kristensen et al., 2013) and the Holocene cooling (e.g., Duplessy et al., 2001, 2005; Risebrobakken et al., 2010, 2011). Potential error

: " Disclaimer: This is a pre-publication version. Readers are recommended to consult the full published version for accuracy and citation."

sources that could impact the accuracy and applicability of both methods also require discussion, such as the possibility of differential degradation of HBIs based on their variable degree of unsaturation (Rontani et al., 2014a, 2018a). To achieve this, in the current study we assessed the agreement of $P_{III}IP_{25}$-based SpSIC estimates (Smik et al., 2016) and CT model predictions (Köseoğlu et al., 2018) in three marine sediment cores located at sites of contrasting contemporary sea ice conditions in the Barents Sea (Fig. 2) and spanning periods of both abrupt and gradual climate shifts throughout the last ca. 16 cal kyr BP. The core sites were chosen based on the availability of previous climatological reconstructions (Cabedo-Sanz et al., 2013; Berben et al., 2014, 2017), a comprehensive suite of HBI concentrations (Belt et al., 2015), and surface sediment-based regional calibrations for both $P_{III}IP_{25}$ and CT approaches (Smik et al., 2016; Köseoğlu et al., 2018). This allowed us to readily identify the causes of discrepancies between the two methods and provide recommendations regarding their complementary application to downcore records.

## 2. Regional setting

The Barents Sea is a seasonally ice-covered shelf area of the Arctic Continental Shelf, which experiences extensive seasonal sea ice cover in winter (October–March) and remains almost entirely ice-free in September following the insolation-induced summer melt (May–August; Sakshaug et al., 2009). It is also characterised by phytoplankton blooms occurring in the highly-productive Marginal Ice Zone (MIZ) along the receding sea ice edge (e.g., Wassmann et al., 1999). The steep salinity and temperature gradients created through mixing of Atlantic Water (AW) and Arctic Water (ArW) mark the position of the Polar Front (PF) and define the winter maximum sea ice extent. The PF position is relatively stable in the western and central Barents Sea (Loeng and Drinkwater, 2007), but becomes more variable to the east where it is characterised by separate temperature and salinity gradients (Oziel et al.,

: " Disclaimer: This is a pre-publication version. Readers are recommended to consult the full published version for accuracy and citation."

2016). Most of the inter-annual sea ice variability occurs in winter and is largely dictated by the volume and temperature of inflowing AW (e.g., Loeng et al., 1997; Smedsrud et al., 2010). While most of the Atlantic-derived heat energy is lost to the atmosphere (Smedsrud et al., 2010, 2013), the volume and temperature of AW inflow have been increasing due to forcing from atmospheric circulation modes, such as the North Atlantic Oscillation (e.g., Loeng et al., 1997; Vinje, 2001; Ingvaldsen et al., 2004; Sorteberg and Kvingedal, 2006), and further amplification via positive feedback mechanisms, including the ice-albedo feedback (Smedsrud et al., 2013). Strengthening of AW inflow has been linked to the diminishing sea ice extent and increasing temperature of the Barents Sea, and continued 'Atlantification' of the region could influence its capacity to limit heat flux to the central Arctic Ocean and hinder sequestration of atmospheric $CO_2$ by halting deep water formation (Screen and Simmonds, 2010; Årthun et al., 2012).

## 3. Materials and methods

### *3.1 Sediment material*

Three sediment cores from sites characterised by different modern sea ice conditions in the Barents Sea were selected for this study. Specific descriptions of all core locations and chronologies are available elsewhere (Ebbesen and Hald, 2004; Rüther et al., 2012; Berben et al., 2014, 2017; Belt et al., 2015). Core NP05-11-70GC (78.67°N, 32.70°E; 293 m water depth), hereafter referred to as core 70, was collected from the Olga Basin to the South of Kong Karls Land (East Svalbard) aboard the *RV Lance* in August of 2005. Core chronology is based on three calibrated $^{14}C$ Accelerated Mass Spectrometry (AMS) dates from mixed foraminifera (Berben et al., 2017). Concentrations of $IP_{25}$ and HBI III (Z) (Fig. 1), $P_{III}IP_{25}$ indices, and associated semi-quantitative SpSIC estimates of core 70 for the last ca. 9.4 cal kyr BP were presented previously (Belt et al., 2015; Berben et al., 2017). Core JM09-KA11-

: " Disclaimer: This is a pre-publication version. Readers are recommended to consult the full published version for accuracy and citation."

GC (74.87°N, 16.48°E; 345 m water depth), hereafter referred to as core 11, was obtained from the Kveithola Trough (South off Svalbard) aboard *RV Jan Mayen* in 2009. We use the age model spanning ca. 16 cal kyr BP presented in Belt et al. (2015) and based on merged $^{14}C$ AMS dates from previous studies (Rüther et al., 2012; Berben et al., 2014). Micropaleontological distributions, stable isotope analyses (Dylmer et al., 2013; Groot et al., 2014), $IP_{25}$ and HBI III (Z) concentrations (and $P_{III}IP_{25}$ values) were presented previously for core 11 (Belt et al., 2015), but not SpSIC estimates. Piston core JM99-1200 (69.27°N, 16.42°E; 475 m water depth), hereafter referred to as core 1200, was retrieved from Andfjorden (northern Norway) aboard the *RV Jan Mayen* in November 1999. Herein, we used the age model of Cabedo-Sanz et al. (2013) corresponding to ca. 14.0–7.0 cal kyr BP (Bølling-Allerød to middle Holocene). Concentrations of $IP_{25}$ and HBI III (Z) and $P_{III}IP_{25}$ values (but not $P_{III}IP_{25}$-derived SpSICs) of core 1200 were reported previously (Cabedo-Sanz et al., 2013; Belt et al., 2015), in addition to sedimentological, isotopic and micropaleontological analyses (Knies et al., 2003; Ebbesen and Hald, 2004). The CT model outputs for cores 70, 11 and 1200 are presented here for the first time.

### *3.2 Proxy and statistical methods*

Modern SpSIC (April-June average for the 1988–2007 period) for each core site was inferred from the Nimbus-7 SMMR and DMSP SSM/I-SSMIS satellite dataset (Cavalieri et al., 1996) used for $PIP_{25}$ and CT model calibrations (Xiao et al., 2015a; Smik et al., 2016; Köseoğlu et al., 2018). Previously published concentrations of $IP_{25}$ and HBI III (Z) for cores 1200 (Cabedo-Sanz et al., 2013) and 11 (Belt et al., 2015) were re-examined to calculate $P_{III}IP_{25}$ indices (Eq. 1; Müller et al., 2011) and derive SpSIC estimates (Eq. 2) using the regional *c*-factor ($c$ = 0.63) and $P_{III}IP_{25}$–SpSIC calibration of Smik et al. (2016), respectively. Additionally, a threshold $P_{III}IP_{25}$ value of 0.8, corresponding to a SpSIC of 68% (Eq. 2), was

: " Disclaimer: This is a pre-publication version. Readers are recommended to consult the full published version for accuracy and citation."

used to indicate the occurrence of at least some (>5%) sea ice cover during the summer months (July–September; Smik et al., 2016). Absolute concentrations (ng/g dry sed.) are denoted by square brackets in all equations.

$$P_{III}IP_{25} = \frac{[IP_{25}]}{([IP_{25}] + [HBI\ III\ (Z)] \times 0.63)} \#(\text{Eqn. 1})$$

$$SpSIC\ (\%) = \frac{(P_{III}IP_{25} - 0.0692)}{0.0107} \#(\text{Eqn. 2})$$

Previously obtained chromatographic and mass spectrometric (MS) data were re-examined to quantify additional HBI lipids (viz. HBIs II and III (E)) required to obtain CT model predictions of sea ice conditions following the method of Köseoğlu et al. (2018). Briefly, percentage abundances of $IP_{25}$ and HBIs II, III (Z) and III (E) (Fig. 1) to their totals were calculated for each core horizon from absolute concentrations (ng/g dry sed.) using Eq. 3.

$$HBI\ (\%) = \frac{[HBI]}{\sum([IP_{25}], [HBI\ II], [HBI\ III\ (Z)], [HBI\ III\ (E)])} \times 100\ \#(\text{Eqn. 3})$$

Subsequently, the CT model constructed from a Barents Sea surface sediment dataset via the R Statistical Package (R Core Team, 2017) was used to classify each core horizon into one of three classes representing marginal (<10% satellite SpSIC), intermediate (10–50% SpSIC), and extensive (>50% SpSIC) spring sea ice conditions. The performance metrics of the CT model used for classification of core horizons are shown in Supplementary Table S1 (Köseoğlu et al., 2018). Biomarker concentrations, $P_{III}IP_{25}$-derived SpSIC and CT model outcomes for all cores are available at https://doi.pangaea.de/10.1594/PANGAEA.891102.

Additional statistical analyses were carried out to supplement the comparison of CT and $P_{III}IP_{25}$-based sea ice assessments. Thus, Pearson's correlations for $IP_{25}$ versus HBI II and HBI III (Z) versus HBI III (E) were calculated from surface sediment data (Fig. 2; Köseoğlu et al., 2018). The biomarker pairings for correlation were chosen due to previous evidence of co-production of sympagic $IP_{25}$ and HBI II (Navarro-Rodriguez et al., 2013; Brown et al.,

: " Disclaimer: This is a pre-publication version. Readers are recommended to consult the full published version for accuracy and citation."

2014, Belt et al., 2016), pelagic HBIs III (Z) and III (E) (Belt et al., 2000; Rowland et al., 2001), as well as significant correlation of these biomarker pairs in the Barents Sea and other Arctic regions (Navarro-Rodriguez et al., 2013; Navarro-Rodriguez, 2014). Thus, the product-moment correlation coefficient was used as a measure of correlation to distinguish between negative and positive linear relationships and identify periods of anomalously deteriorated correlations in downcore records compared to those characteristic of relatively modern settings represented by surface sediments. Further, rolling Pearson's correlations were calculated for all downcore records using a sampling window of nine, corresponding to a time window of between ca. 0.5–2.0 cal kyr BP. All correlation and CT model analyses were incorporated into functions within the R statistical package (R Core Team, 2017). The source code and supporting materials are available at https://doi.org/10.5281/zenodo.1346305.

## 4. Results and Discussion

The applicability of multivariate CT models and $P_{III}IP_{25}$-based semi-quantitative SpSIC estimates (Eq. 1 and 2) as complementary methods for sea ice reconstruction spanning both abrupt and gradual climate shifts of the Younger Dryas and Holocene (ca. last 13.0 cal kyr BP) was assessed by comparing the results of both approaches in cores 11, 70 and 1200 (Figs. 3–6). The assessment of consistency between the two methods was contextualised further by considering findings of previous studies (e.g., Belt et al., 2015).

### *4.1 Core 70 (northern Barents Sea)*

The core 70 site is characterised by extensive modern sea ice conditions (≈80% SpSIC) and the downcore record represents a gradual evolution of sea ice cover in the

: “ Disclaimer: This is a pre-publication version. Readers are recommended to consult the full published version for accuracy and citation.”

northern Barents Sea from ice-free conditions during the early Holocene to prolonged seasonal sea ice presence prevalent in the region today. The primarily insolation-controlled southward expansion of sea ice cover previously inferred for the core site throughout the Holocene (Belt et al., 2015; Berben et al., 2017) is reflected in the CT model assessment (Fig. 3). Consistent with the onset of the Holocene Thermal Maximum and the resulting proximity of the annual maximum sea ice edge to the core site between ca. 9.5–8.5 cal kyr BP evident from low $P_{III}IP_{25}$-derived SpSIC (ca. 5–15%), the CT model predicts mostly marginal sea ice conditions during this interval. Similarly, the southward migration of sea ice beginning ca. 8.5 cal kyr BP as a response to decreasing summer insolation (Berben et al., 2017) is also reflected by a switch of CT model assessment from marginal to intermediate sea ice conditions. Finally, following a period of consistent intermediate ice conditions (ca. 30 ± 4 % SpSIC), a further southward migration of the ice edge between ca. 6.5–5.9 cal kyr BP, previously attributed to further decreasing solar insolation and reduced AW influence (Berben et al., 2017), is reflected by an associated shift of CT model predictions from intermediate to extensive sea ice conditions at ca. 6.0 cal kyr BP. This trend agrees with previous reports of Neoglaciation in the Barents Sea, a period characterised by glacier advances and increased sea ice export via the Fram Strait when modern-type oceanic circulation was re-established (Werner et al., 2013, 2016; Rasmussen and Thomsen, 2015).

Overall, the timing of CT prediction shifts was consistent with previously inferred climate evolution at the core 70 site (Berben et al., 2017), and no discrepancies from semi-quantitative SpSIC estimates were observed (Fig. 3), with all horizons consistently classified within the satellite SpSIC boundaries defined in the CT model training set (Fig. 2). Our data supports the complementary application of both approaches when describing gradual changes in sea ice conditions at millennial timescales, where CT predictions have the potential to identify the timing of switches between distinct sea ice conditions, as hypothesized

: " Disclaimer: This is a pre-publication version. Readers are recommended to consult the full published version for accuracy and citation."

previously (Köseoğlu et al., 2018). However, we note that the CT model is limited by the class boundaries assigned to the training set (Fig. 2), which may result in insufficiently detailed assessment of changing sea ice conditions. In this case, a distinct ice expansion ca. 2.7 cal kyr BP (SpSIC values of <80%; Fig. 3b) previously linked to insolation decreases (Berben et al., 2017) was not identified by the CT model since the 50–100% SpSIC range is only represented by a single class within the training set (Fig. 2). Such limitations of the training set, in this case driven by reduced sample density around Svalbard, should be considered when interpreting model output. The otherwise high agreement with the $P_{III}IP_{25}$ approach is potentially attributable, at least in part, to significantly similar HBI distributions and data structure between the surface sediment training set and core 70. Like most supervised classification methods, CTs rely on distributional similarity of predictive variables (e.g., HBI percentages) between the training set and new samples to be classified. Thus, in our study, the model is only likely to function correctly when the overall relative abundance ranges and relationships between HBIs observed in the surface sediment training set (Fig. 2) are reproduced in downcore records. This is the case for core 70, where consistently significant positive correlations are observed for $IP_{25}$ versus HBI II and HBI III (Z) versus HBI III (E) biomarker pairs (Fig. 3c), also evident in surface sediments with different overlying SpSIC (Fig. 7) used to build the CT model. Relative HBI abundances (Eq. 3) are also comparable and generally dominated by sympagic biomarkers in both datasets (Fig. 8); although we stress that inherent HBI variability in surface sediments and core 70 prevent any detailed interpretation of spatially and temporally averaged values. Nonetheless, such visualisations of data ranges and structure help inform the expected CT performance for a given dataset and suggest that the model is likely to perform well for core 70.

### *4.2 Core 1200 (southwestern Barents Sea)*

: " Disclaimer: This is a pre-publication version. Readers are recommended to consult the full published version for accuracy and citation."

311 In contrast to contemporary ice-free conditions that characterise the core 1200 site, harsh
312 glacial conditions with short ice-free summers during the majority of the Younger Dryas cold
313 stadial spanning ca.13.0–11.9 cal kyr BP were previously inferred (Cabedo-Sanz et al., 2013;
314 Belt et al., 2015). Accordingly, our records show elevated $P_{III}IP_{25}$-derived SpSIC values
315 (>75%) accompanied by CT model predictions of extensive sea ice conditions during this
316 period (Fig. 4b–c). Subsequently, ameliorated conditions are evident during the Younger
317 Dryas–Holocene transition, with precipitous decrease of SpSIC estimates (to ca. 10–40%)
318 and a switch of CT model assessment from extensive to marginal (<10% SpSIC) sea ice
319 conditions. In core 1200, the ice retreat is characterised by rapid fluctuations of SpSIC
320 estimates, consistent with switching of CT model assessment between intermediate and
321 marginal classification of sea ice cover during the 11.9–11.5 cal kyr BP period, which is
322 followed by ice-free conditions for the remainder of the record (Fig. 4b). Similar unstable
323 conditions, likely attributable to the return of thermohaline circulation during this period
324 (e.g., Bakke et al., 2009), were previously inferred for core 1200 from $PIP_{25}$ records (Cabedo-
325 Sanz et al., 2013; Belt et al., 2015), as well as sea surface temperature (SST) and sea surface
326 salinity (SSS) reconstructions based on stable isotope measurements of planktic foraminifera
327 (Ebbesen and Hald, 2004).

328 The apparent consistency of CT predictions and $P_{III}IP_{25}$-derived SpSIC in core 1200
329 suggests that both methods respond similarly to extremes of sea ice conditions observed both
330 during (ca. 13.0–12.0 cal kyr BP) and after (11.5 cal kyr BP onwards) the Younger Dryas
331 stadial. However, while the CT model also detected rapid fluctuations of sea ice cover during
332 the climatically unstable YD–Holocene transition (11.9–11.5 cal kyr BP), several horizons (n
333 = 7) were classified outside of the categorical sea ice boundaries based on satellite SpSIC
334 thresholds (Fig. 2 and 3b). Nonetheless, such discrepancies with the $P_{III}IP_{25}$-based SpSIC
335 record were always within the RMSE of the regional $P_{III}IP_{25}$–SpSIC calibration (ca. ±11%

: " Disclaimer: This is a pre-publication version. Readers are recommended to consult the full published version for accuracy and citation."

SpSIC; Smik et al., 2016), and are potentially attributable to various error sources associated with $P_{III}IP_{25}$-based SpSIC estimates and CT models. For example, the dependence of $P_{III}IP_{25}$ values on the *c*-factor may significantly influence the regional comparability of the resulting SpSIC estimates. While the general trends of $P_{III}IP_{25}$-derived SpSIC were previously shown to be unaffected by the magnitude of the *c*-factor (Belt et al., 2015; Smik et al., 2016), $P_{III}IP_{25}$ values (and associated SpSIC estimates; Eq. 1 and 2) may vary by ca. 10% when omitting the *c*-factor ($c$ = 1; Smik et al., 2016). Further, the *c*-factor used in the current study ($c$ = 0.63; Eq. 1) was calculated based on average $IP_{25}$ and HBI III (Z) concentrations from a wide range of Barents Sea locations characterised by different sea ice conditions (Smik et al., 2016). Thus, the regional applicability of a spatially averaged *c*-factor remains a challenge, and the same value may not provide fully comparable SpSIC estimates for all downcore locations in our study. In contrast, the CT approach is based on a multivariate set of HBI biomarkers, is therefore independent of the *c*-factor, and probably provides results that are more comparable between locations within the geographical coverage of the surface sediment dataset used for model training (Köseoğlu et al., 2018). Together, these caveats imply that the interpretation of $P_{III}IP_{25}$-derived SpSIC variability and any discrepancies with CT model predictions within the associated RMSE (±11 % SpSIC) should be avoided, and broader changes beyond this error range should instead be considered. Additionally, unlike core 70, the data structure in core 1200 is significantly unstable during rapid climate fluctuations, with correlations degrading to near-zero values (Fig. 4c). This potentially hinders CT performance due to unpredictable data structure differences with the surface sediment training set. The CT model was previously shown to lose performance (with a ca. 20% misclassification error; Supplementary Table S1) in areas characterised by highly variable sea ice and primary productivity regimes, such as the MIZ of western Svalbard and the central Barents Sea. The period of high misclassification spanning 11.9–11.5 cal kyr BP in core 1200 was

: “ Disclaimer: This is a pre-publication version. Readers are recommended to consult the full published version for accuracy and citation.”

characterised by the return of enhanced biogenic production (Knies, 2005), fluctuating AW inflow, and similarly variable sea ice conditions resulting from meltwater and nutrient input from waning ice sheets (Cabedo-Sanz et al., 2013). It is possible that CT performance suffered during this interval of significantly unstable sea ice cover and primary productivity regimes, of which the latter could potentially have contributed to degraded correlations observed in our record (Fig. 4c) due to inconsistent, variable HBI production. Overall, our results suggest that CT predictions potentially become more prone to misclassification, and therefore less consistent with semi-quantitative SpSIC estimates, in rapidly shifting climate conditions observed during stadial-interstadial transitions. Finally, misclassification errors may also be associated with information loss due to insufficient representation of the SpSIC range (0–100%) in the CT model. Specifically, the surface sediment dataset used for model construction contains no samples with modern overlying SpSIC of 16–22% and 56–67% (Köseoğlu et al., 2018), potentially resulting in an incomplete model definition near the marginal-intermediate (10% satellite SpSIC) and intermediate-extensive (50% satellite SpSIC) sea ice class boundaries, respectively. Such potential error sources may be mitigated by expansion of the model training set to increase sample density and include such under-represented SpSIC ranges. In the meantime, we suggest that shifts in CT model class predictions should be interpreted as broader changes between sea ice regimes, rather than between definitive SpSIC threshold values. Thus, the marginal, intermediate, and extensive sea ice classes included in the model (Fig. 2) likely represent ice-free or proximal maximum ice edge conditions, the highly-productive MIZ during the spring melt season, and more northern regions where ice cover persists until ca. August–September (e.g., North-East of Svalbard), respectively.

### *4.3 Core 11 (western Barents Sea)*

: " Disclaimer: This is a pre-publication version. Readers are recommended to consult the full published version for accuracy and citation."

386 The core 11 site in our dataset is presently characterised by marginal SpSIC (<5%)
387 with a proximal spring sea ice edge (Fig. 2). As seen for core 1200, the site experienced
388 SpSIC values of ca. 80% during the Younger Dryas (ca. 13.0–12.0 cal kyr BP), but exhibited
389 a more gradual ice retreat and a step-wise switch of CT model predictions from extensive
390 towards marginal sea ice conditions during the 12.0–11.5 cal kyr BP period (Fig. 5b). A
391 period of highly unstable sea ice cover is instead observed between ca. 11.0–10.0 cal kyr BP,
392 with fluctuating SpSIC estimates (ca. 0–65%) and CT model predictions. This is consistent
393 with the return of enhanced sub-surface AW inflow to the core site after ca. 11.5 cal kyr BP
394 inferred from benthic foraminiferal census data (Groot et al., 2014), with a contrastingly
395 colder surface water layer dominated by ArW inferred from reduced SSTs (Berben et al.,
396 2014). From ca. 10.0–1.5 cal kyr BP, ice-free conditions characterised the core 11 site, as
397 evidenced by consistently low SpSIC (ca. <10%) and marginal sea ice conditions predicted
398 by the CT model, and further supported by an enhancement of AW inflow to the core site
399 from ca. 9.8 cal kyr BP (Groot et al., 2014). Finally, re-emergence of highly fluctuating sea
400 ice cover during the last ca. 0.9–0.6 cal kyr BP (Berben et al., 2014; Belt et al., 2015), despite
401 increasing AW inflow (Dylmer et al., 2013), was also captured by the CT model, which
402 switches from marginal to intermediate sea ice conditions at this time (Fig. 5b).

403 Consistent with outcomes from core 1200, several horizons (n = 20) from core 11
404 were classified outside of the sea ice class boundaries based on satellite SpSIC thresholds.
405 Notably, these differences also exceeded the standard RMSE (±11% SpSIC) of the regional
406 $P_{III}IP_{25}$-SpSIC calibration (Eq. 2; Smik et al., 2016) for four horizons, where marginal sea ice
407 cover (<10% satellite SpSIC) was inferred for $P_{III}IP_{25}$-derived SpSIC values in excess of ca.
408 40% (Fig. 5b). Most significant misclassification was observed during periods of high
409 climatic variability (11.5–10.0 and 0.9–0.6 cal kyr BP), consistent with the return of variable
410 sub-surface AW inflow. As with core 1200, we suggest that this stems from considerably

: “ Disclaimer: This is a pre-publication version. Readers are recommended to consult the full published version for accuracy and citation.”

411 different distributions and data structure of HBIs in the misclassified horizons compared to
412 those of surface sediments used for model construction, potentially caused by climate
413 fluctuations during intervals of rapid climate change. Indeed, running correlations between
414 $IP_{25}$ and HBI II severely degrade towards negative *r* values during the 11.5–10.0 cal kyr BP
415 interval and the last 0.7 cal kyr BP (Fig. 5c), thus deviating from the consistently high
416 positive associations observed in the surface training set (Fig. 7). Indeed, these distributional
417 changes coincide with CT misclassification beyond the $P_{III}IP_{25}$-based SpSIC error of 11% and
418 are better illustrated when considering individual concentration profiles of $IP_{25}$ and HBI II, as
419 well as rolling correlations of corresponding relative differences (Fig. 6). It is evident that
420 disproportional increases of HBI II relative to $IP_{25}$ contribute to the correlation reduction.
421 Similar increases in the HBI II/$IP_{25}$ ratio were previously observed across the Arctic during
422 periods of increased warm water inflow from the North Atlantic and North Pacific (e.g., Fahl
423 and Stein, 2012; Hörner et al., 2016; Ruan et al., 2017), conditions that also characterised the
424 core 11 site during intervals of elevated HBI II concentration (Berben et al., 2014; Belt et al.,
425 2015). Overall, our data support the results from core 1200 and suggest that CT performance
426 and consistency with the $P_{III}IP_{25}$ approach suffer when HBI distributions included in the
427 model training set are not represented in downcore records characterised by different or
428 unstable climate. Visualisation of the variables used in the CT assessment (Fig. 5 and 6) is
429 essential when identifying such cases. It is important to acknowledge that this limitation is
430 potentially amplified as variations in relative abundances of any biomarker included in the
431 model inherently affect the overall HBI composition due to data normalisation used for the
432 CT (Eq. 3). The dependence of CT performance and viability on the consistency of data
433 distribution in the training set with that of new samples highlights the necessity of
434 constructing separate training sets for different Arctic regions, which often exhibit
435 significantly different HBI distributions despite similar seasonal ice conditions (Stoynova et

: " Disclaimer: This is a pre-publication version. Readers are recommended to consult the full published version for accuracy and citation."

al., 2013; Xiao et al., 2015a). Ideally, downcore records to be classified should be within the geographical coverage of the surface sediment training set, as is the case in our study. Further, the choice of an optimal time interval for the satellite SpSIC data is potentially problematic due to the often unavailability of accumulation rates for surface sediments. Thus, the integrated biomarker signal at each surface location potentially corresponds to a variable temporal window (Köseoğlu et al., 2018) and some surface sediments may not even represent recent accumulation. This is likely to influence the accuracy of both the CT model and $P_{III}IP_{25}$-based SpSIC estimates.

Another important consideration is the consistent quantification of all biomarkers between the training set and new samples. Accurate quantification of HBIs via mass spectrometric techniques involves the use of an instrumental Response Factor (RF), usually obtained from calibration with authentic standards, to account for mass spectral fragmentation efficiency differences between individual biomarkers and the internal standard (Belt et al., 2012; Belt et al., 2014). Moreover, HBIs usually exhibit vastly different RF values (Belt et al., 2014), necessitating instrument calibration via separate standard series for each biomarker and subsequent quality monitoring using a reference sediment material of known HBI concentration. Any RF changes thus affect the HBI distribution and resulting CT model rules, such that the use of different quantification methods (RF values) for the model training set and new samples will cause the model to fail when classifying the latter. For our data, assigning the same value to all RFs shifts the HBI composition towards higher relative abundances of HBI III (Z) and HBI III (E) (Fig. 8a). When these modified downcore distributions are classified using the CT model trained with correctly quantified surface sediments (Köseoğlu et al., 2018), the model fails to identify the extensive sea ice class completely and exhibits a high discrepancy with $P_{III}IP_{25}$-based SpSIC. On the other hand, when consistent methods are used to obtain the RFs, model performance is largely unaffected

: " Disclaimer: This is a pre-publication version. Readers are recommended to consult the full published version for accuracy and citation."

(Fig. 8b). Directly comparable quantification is therefore necessary for the training and new sample sets, and the CT must be re-built with a new training set should a change in quantification methods occur.

Finally, the relatively high susceptibility of more unsaturated HBIs, particularly those with trisubstituted double bonds (HBIs III (Z) and III (E) in this case), towards degradative processes could also alter biomarker distributions in downcore sedimentary sequences relative to those in surface sediments. The lower stability of HBI trienes towards photodegradation and autoxidation in sea ice and the water column (Rontani et al., 2014a,b) possibly implies their increased potential for aerobic degradation in upper oxic sediments, which was shown recently to affect even the more diagenetically stable $IP_{25}$ (Rontani et al., 2018a,b). Thus, selective removal of HBIs III (Z) and III (E) from the HBI distribution may adversely affect $P_{III}IP_{25}$-based SpSIC estimates and CT model performance, especially under conditions of high light penetration, long residence times of algal cells in the photic zone, and low sedimentation rates, where diagenetic processes are more likely to have an effect. While it is not feasible to analytically diagnose the relative impacts of climate change and selective HBI degradation due to the extremely high reactivity of associated photo- and oxidation products (Rontani et al., 2014a,b), examination of HBI triene concentration profiles suggests a prevailing influence of climate on our data. Specifically, the concentrations of pelagic HBI III (Z) reach and surpass those of $IP_{25}$ (Fig. 3a, 4a, and 5a) during periods of reduced sea ice cover and generally ameliorated climate conditions inferred in previous studies, while reduced concentrations only coincide with harsh glacial conditions of the Younger Dryas and the late Holocene ice expansion (Cabedo-Sanz et al., 2013; Berben et al., 2014, 2017). Moreover, downcore concentrations of HBIs III (Z) and III (E) are often higher than maximum values observed in surface sediments from the highly-productive MIZ, which are ca. 40 ng/g and 20 ng/g for HBIs III (Z) and III (E), respectively (Köseoğlu et al., 2018). This

: " Disclaimer: This is a pre-publication version. Readers are recommended to consult the full published version for accuracy and citation."

suggests that, in this case, sedimentary aerobic degradation or other processes prior to deposition are unlikely to significantly alter downcore HBI content relative to that of proximal surface sediments. Finally, as noted previously, the alteration of HBI distributions and data structure due to disproportional and even opposing concentration increases of II relative to those of $IP_{25}$ is the likely cause of discrepancies between $P_{III}IP_{25}$- and CT-based methods for cores 1200 and 11, in particular (Fig. 4–6). Nonetheless, a diagenetic influence on downcore HBI concentrations cannot be discounted, particularly in older core sections or when overlying climate conditions are more likely to promote accelerated or prolonged oxidation and photodegradation. Thus, we suggest that HBI distributions should be combined with degradation proxies, such as the recently utilized ratio of brassicasterol to 24-methylenecholesterol (Rontani et al., 2018a), and that uncharacteristically low concentrations of HBIs III (Z) and III (E) relative to otherwise inferred climate conditions (e.g., using other proxies) should be interpreted with caution.

## 5. Conclusions

Downcore records encompassing different modern sea ice conditions in the Barents Sea were used to assess the spatio-temporal consistency between CT model predictions and $P_{III}IP_{25}$-based SpSIC estimates. A good overall agreement between both approaches was observed for all cores, and the CT model was able to capture both abrupt and fluctuating shifts in sea ice regimes, such as those evident during the Younger Dryas stadial, as well as more gradual trends in sea ice conditions during the Holocene. However, shifts of CT model predictions occurred at variable threshold values of $P_{III}IP_{25}$-based SpSIC estimates in different downcore records (ca. ±11% for 16 samples, >11% for 4 samples). This variability was attributed partially to the occurrence of downcore HBI distributions, which are not

: “ Disclaimer: This is a pre-publication version. Readers are recommended to consult the full published version for accuracy and citation.”

represented in the model training dataset, most notably during intervals of unstable and rapid climate change characterising stadial-interstadial transitions. While it is not feasible to avoid this limitation, examination of data structure and distribution may pinpoint intervals where CT performance is likely to decrease. A consequence of CT dependency on HBI distributional changes is the necessity to use consistent quantification methods for model training and new (downcore) samples, and to use separate training sets for different Arctic regions. Selective removal of more unsaturated HBIs via degradation processes represents another potential error source, although this was likely not the case for our data. Further potential error sources of both methods were also identified, including the uncertain regional applicability of a uniform *c*-factor and insufficient sample density for representation of the entire SpSIC range (0–100%) within the CT model. We suggest, therefore, that only variations of $P_{III}IP_{25}$-based SpSIC exceeding the associated RMSE of 11% be considered significant, and that CT model predictions should be interpreted in terms of broader changes in sea ice regimes (i.e. open water or proximal ice edge, MIZ conditions, and stable sea ice cover) rather than inflexible satellite-based numeric SpSIC thresholds (i.e. 10% and 50% SpSIC).

## Acknowledgments

This work was jointly supported by the University of Plymouth and the Research Council of Norway through its Centre of Excellence funding scheme for CAGE, (project 223259). We thank Yunping Xu and an anonymous reviewer for providing valuable comments that improved the overall quality of the manuscript.

: " Disclaimer: This is a pre-publication version. Readers are recommended to consult the full published version for accuracy and citation."

## 6. References

Andrews, J.T., Belt, S.T., Olafsdottir, S., Massé, G., Vare, L.L., 2009. Sea ice and marine climate variability for NW Iceland/Denmark Strait over the last 2000 cal. yr BP. The Holocene 19, 775-784.

Årthun, M., Eldevik, T., Smedsrud, L.H., Skagseth, Ø., Ingvaldsen, R.B., 2012. Quantifying the influence of Atlantic heat on Barents Sea ice variability and retreat. Journal of Climate 25, 4736-4743.

Axford, Y., Andresen, C.S., Andrews, J.T., Belt, S.T., Geirsdóttir, Á., Massé, G., Miller, G.H., Ólafsdóttir, S., Vare, L.L., 2011. Do paleoclimate proxies agree? A test comparing 19 late Holocene climate and sea-ice reconstructions from Icelandic marine and lake sediments. Journal of Quaternary Science 26, 645-656.

Bakke, J., Lie, Ø., Heegaard, E., Dokken, T., Haug, G.H., Birks, H.H., Dulski, P., Nilsen, T., 2009. Rapid oceanic and atmospheric changes during the Younger Dryas cold period. Nature Geoscience 2, 202-205.

Bartels, M., Titschack, J., Fahl, K., Stein, R., Seidenkrantz, M.S., Hillaire-Marcel, C., Hebbeln, D., 2017. Atlantic Water advection vs glacier dynamics in northern Spitsbergen since early deglaciation. Climate of the Past Discussions 2017, 1-53.

Belt, S.T., Müller, J., 2013. The Arctic sea ice biomarker $IP_{25}$: a review of current understanding, recommendations for future research and applications in palaeo sea ice reconstructions. Quaternary Science Reviews 79, 9-25.

Belt, S.T., Allard, W.G., Massé, G., Robert, J.-M., Rowland, S.J., 2000. Highly branched isoprenoids (HBIs): identification of the most common and abundant sedimentary isomers. Geochimica et Cosmochimica Acta 64, 3839-3851.

: " Disclaimer: This is a pre-publication version. Readers are recommended to consult the full published version for accuracy and citation."

558 Belt, S.T., Massé, G., Rowland, S.J., Poulin, M., Michel, C., LeBlanc, B., 2007. A novel
559 chemical fossil of palaeo sea ice: $IP_{25}$. Organic Geochemistry 38, 16-27.
560 Belt, S.T., Brown, T.A., Rodriguez, A.N., Sanz, P.C., Tonkin, A., Ingle, R., 2012. A
561 reproducible method for the extraction, identification and quantification of the Arctic
562 sea ice proxy $IP_{25}$ from marine sediments. Analytical Methods 4, 705-713.
563 Belt, S.T., Brown, T.A., Ringrose, A.E., Cabedo-Sanz, P., Mundy, C.J., Gosselin, M., Poulin,
564 M., 2013. Quantitative measurement of the sea ice diatom biomarker $IP_{25}$ and sterols
565 in Arctic sea ice and underlying sediments: Further considerations for palaeo sea ice
566 reconstruction. Organic Geochemistry 62, 33-45.
567 Belt, S.T., Brown, T.A., Ampel, L., Cabedo-Sanz, P., Fahl, K., Kocis, J.J., Massé, G.,
568 Navarro-Rodriguez, A., Ruan, J., Xu, Y., 2014. An inter-laboratory investigation of
569 the Arctic sea ice biomarker proxy $IP_{25}$ in marine sediments: key outcomes and
570 recommendations. Climate of the Past 10, 155-166.
571 Belt, S.T., Cabedo-Sanz, P., Smik, L., Navarro-Rodriguez, A., Berben, S.M.P., Knies, J.,
572 Husum, K., 2015. Identification of paleo Arctic winter sea ice limits and the marginal
573 ice zone: optimised biomarker-based reconstructions of late Quaternary Arctic sea ice.
574 Earth and Planetary Science Letters 431, 127-139.
575 Belt, S.T., Smik, L., Brown, T.A., Kim, J.H., Rowland, S.J., Allen, C.S., Gal, J.K., Shin,
576 K.H., Lee, J.I., Taylor, K.W.R., 2016. Source identification and distribution reveals
577 the potential of the geochemical Antarctic sea ice proxy $IPSO_{25}$. Nature
578 Communications 7, 12655. DOI: https://doi.org/10.1038/ncomms12655.
579 Belt, S.T., Brown, T.A., Smik, L., Tatarek, A., Wiktor, J., Stowasser, G., Assmy, P., Allen,
580 C.S., Husum, K., 2017. Identification of $C_{25}$ highly branched isoprenoid (HBI)
581 alkenes in diatoms of the genus *Rhizosolenia* in polar and sub-polar marine
582 phytoplankton. Organic Geochemistry 110, 65-72.

: " Disclaimer: This is a pre-publication version. Readers are recommended to consult the full published version for accuracy and citation."

583 Belt, S.T., Brown, T.A., Smik, L., Assmy, P., Mundy, C.J., 2018. Sterol identification in
584 floating Arctic sea ice algal aggregates and the Antarctic sea ice diatom *Berkeleya*
585 *adeliensis*. Organic Geochemistry 118, 1-3.
586 Berben, S.M.P., Husum, K., Cabedo-Sanz, P., Belt, S.T., 2014. Holocene sub-centennial
587 evolution of Atlantic water inflow and sea ice distribution in the western Barents Sea.
588 Climate of the Past 10, 181-198.
589 Berben, S.M.P., Husum, K., Navarro-Rodriguez, A., Belt, S.T., Aagaard-Sørensen, S., 2017.
590 Semi-quantitative reconstruction of early to late Holocene spring and summer sea ice
591 conditions in the northern Barents Sea. Journal of Quaternary Science 32, 587-603.
592 Bitz, C.M., Gent, P.R., Woodgate, R.A., Holland, M.M., Lindsay, R., 2006. The influence of
593 sea ice on ocean heat uptake in response to increasing $CO_2$. Journal of Climate 19,
594 2437-2450.
595 Breiman, L., Friedman, J., Stone, C.J., Olshen, R.A., 1984. Classification and regression
596 trees. CRC press, New York, ISBN: 9780412048418.
597 Brown, T.A., Belt, S.T., Tatarek, A., Mundy, C.J., 2014. Source identification of the Arctic
598 sea ice proxy $IP_{25}$. Nature Communications 5, 4197. DOI:
599 https://doi.org/10.1038/ncomms5197.
600 Cabedo-Sanz, P., Belt, S.T., 2016. Seasonal sea ice variability in eastern Fram Strait over the
601 last 2000 years. Arktos 2, 22. DOI: https://doi.org/10.1007/s41063-016-0023-2.
602 Cabedo-Sanz, P., Belt, S.T., Jennings, A.E., Andrews, J.T., Geirsdóttir, Á., 2016. Variability
603 in drift ice export from the Arctic Ocean to the North Icelandic Shelf over the last
604 8000 years: a multi-proxy evaluation. Quaternary Science Reviews 146, 99-115.
605 Cabedo-Sanz, P., Belt, S.T., Knies, J., Husum, K., 2013. Identification of contrasting seasonal
606 sea ice conditions during the Younger Dryas. Quaternary Science Reviews 79, 74-86.

: “ Disclaimer: This is a pre-publication version. Readers are recommended to consult the full published version for accuracy and citation.”

607 Cavalieri, D.J., Parkinson, C.L., Gloersen, P., Zwally, H.J., 1996. Sea Ice Concentrations
608 from Nimbus-7 SMMR and DMSP SSM/I-SSMIS Passive Microwave Data, ver 1.1.
609 NASA DAAC at the National Snow and Ice Data Center, Boulder, Colorado. DOI:
610 https://doi.org/10.5067/8GQ8LZQVL0VL [Accessed 08.06.2018]
611 Divine, D.V., Dick, C., 2006. Historical variability of sea ice edge position in the Nordic
612 Seas. Journal of Geophysical Research: Oceans 111, C01001. DOI:
613 https://doi.org/10.1029/2004JC002851.
614 Duplessy, J.-C., Ivanova, E., Murdmaa, I., Paterne, M., Labeyrie, L., 2001. Holocene
615 paleoceanography of the northern Barents Sea and variations of the northward heat
616 transport by the Atlantic Ocean. Boreas 30, 2-16.
617 Duplessy, J.C., Cortijo, E., Ivanova, E., Khusid, T., Labeyrie, L., Levitan, M., Murdmaa, I.,
618 Paterne, M., 2005. Paleoceanography of the Barents Sea during the Holocene.
619 Paleoceanography 20, PA4004. DOI: https://doi.org/10.1029/2004PA001116
620 Dylmer, C.V., Giraudeau, J., Eynaud, F., Husum, K., De Vernal, A., 2013. Northward
621 advection of Atlantic water in the eastern Nordic Seas over the last 3000 yr. Climate
622 of the Past 9, 1505-1518.
623 Ebbesen, H., Hald, M., 2004. Unstable Younger Dryas climate in the northeast North
624 Atlantic. Geology 32, 673-676.
625 Eisenman, I., Wettlaufer, J.S., 2009. Nonlinear threshold behavior during the loss of Arctic
626 sea ice. Proceedings of the National Academy of Sciences 106, 28-32.
627 Fahl, K., Stein, R., 2012. Modern seasonal variability and deglacial/Holocene change of
628 central Arctic Ocean sea-ice cover: new insights from biomarker proxy records. Earth
629 and Planetary Science Letters 351-352, 123-133.

: “ Disclaimer: This is a pre-publication version. Readers are recommended to consult the full published version for accuracy and citation.”

630 Fetterer, F., Knowles, K., Meier, W.N., Savoie, M., 2017. Sea Ice Index, in: NSIDC: National
631 Snow and Ice Data Center, ver. 3. NSIDC: National Snow and Ice Data Center,
632 Boulder, Colorado. DOI: https://doi.org/10.7265/N5736NV7 [Accessed 08.06.2018]
633 Groot, D.E., Aagaard-Sørensen, S., Husum, K., 2014. Reconstruction of Atlantic water
634 variability during the Holocene in the western Barents Sea. Climate of the Past 10, 51-
635 62.
636 Harada, N., 2016. Review: Potential catastrophic reduction of sea ice in the western Arctic
637 Ocean: Its impact on biogeochemical cycles and marine ecosystems. Global and
638 Planetary Change 136, 1-17.
639 Hoff, U., Rasmussen, T.L., Stein, R., Ezat, M.M., Fahl, K., 2016. Sea ice and millennial-scale
640 climate variability in the Nordic seas 90 kyr ago to present. Nature Communications
641 7, 12247. DOI: https://doi.org/10.1038/ncomms12247.
642 Hörner, T., Stein, R., Fahl, K., Birgel, D., 2016. Post-glacial variability of sea ice cover, river
643 run-off and biological production in the western Laptev Sea (Arctic Ocean) – A high-
644 resolution biomarker study. Quaternary Science Reviews 143, 133-149.
645 Ingvaldsen, R.B., Asplin, L., Loeng, H., 2004. Velocity field of the western entrance to the
646 Barents Sea. Journal of Geophysical Research: Oceans 109, C03021. DOI:
647 https://doi.org/10.1029/2003JC001811.
648 Knies, J., 2005. Climate-induced changes in sedimentary regimes for organic matter supply
649 on the continental shelf off northern Norway. Geochimica et Cosmochimica Acta 69,
650 4631-4647.
651 Knies, J., Cabedo-Sanz, P., Belt, S.T., Baranwal, S.F., Rosell-Melé, A., 2014. The emergence
652 of modern sea ice cover in the Arctic Ocean. Nature Communications 5, 5608. DOI:
653 https://doi.org/10.1038/ncomms6608.

: “ Disclaimer: This is a pre-publication version. Readers are recommended to consult the full published version for accuracy and citation.”

654 Knies, J., Hald, M., Ebbesen, H., Mann, U., Vogt, C., 2003. A deglacial–middle Holocene
655 record of biogenic sedimentation and paleoproductivity changes from the northern
656 Norwegian continental shelf. Paleoceanography 18, 1096. DOI:
657 https://doi.org/10.1029/2002PA000872.
658 Knies, J., Pathirana, I., Cabedo-Sanz, P., Banica, A., Fabian, K., Rasmussen, T.L., Forwick,
659 M., Belt, S.T., 2017. Sea-ice dynamics in an Arctic coastal polynya during the past
660 6500 years. Arktos 3, 1. DOI: https://doi.org/10.1007/s41063-016-0027-y.
661 Köseoğlu, D., Belt, S.T., Smik, L., Yao, H., Panieri, G., Knies, J., 2018. Complementary
662 biomarker-based methods for characterising Arctic sea ice conditions: A case study
663 comparison between multivariate analysis and the $PIP_{25}$ index. Geochimica et
664 Cosmochimica Acta 222, 406-420.
665 Kristensen, D.K., Rasmussen, T.L., Koç, N., 2013. Palaeoceanographic changes in the
666 northern Barents Sea during the last 16,000 years – new constraints on the last
667 deglaciation of the Svalbard–Barents Sea Ice Sheet. Boreas 42, 798-813.
668 Lindsay, R., Schweiger, A., 2015. Arctic sea ice thickness loss determined using subsurface,
669 aircraft, and satellite observations. The Cryosphere 9, 269-283.
670 Lindsay, R.W., Zhang, J., 2005. The Thinning of Arctic Sea Ice, 1988–2003: Have We
671 Passed a Tipping Point? Journal of Climate 18, 4879-4894.
672 Loeng, H., Drinkwater, K., 2007. An overview of the ecosystems of the Barents and
673 Norwegian Seas and their response to climate variability. Deep Sea Research Part II:
674 Topical Studies in Oceanography 54, 2478-2500.
675 Loeng, H., Ozhigin, V., Ådlandsvik, B., 1997. Water fluxes through the Barents Sea. ICES
676 Journal of Marine Science 54, 310-317.

: “ Disclaimer: This is a pre-publication version. Readers are recommended to consult the full published version for accuracy and citation.”

677 Massé, G., Rowland, S.J., Sicre, M.-A., Jacob, J., Jansen, E., Belt, S.T., 2008. Abrupt climate
678 changes for Iceland during the last millennium: evidence from high resolution sea ice
679 reconstructions. Earth and Planetary Science Letters 269, 565-569.
680 Maykut, G.A., 1978. Energy exchange over young sea ice in the central Arctic. Journal of
681 Geophysical Research: Oceans 83, 3646-3658.
682 Méheust, M., Fahl, K., Stein, R., 2013. Variability in modern sea surface temperature, sea ice
683 and terrigenous input in the sub-polar North Pacific and Bering Sea: reconstruction
684 from biomarker data. Organic Geochemistry 57, 54-64.
685 Meier, W.N., Hovelsrud, G.K., van Oort, B.E.H., Key, J.R., Kovacs, K.M., Michel, C., Haas,
686 C., Granskog, M.A., Gerland, S., Perovich, D.K., Makshtas, A., Reist, J.D., 2014.
687 Arctic sea ice in transformation: a review of recent observed changes and impacts on
688 biology and human activity. Reviews of Geophysics 52, 185-217.
689 Mori, M., Watanabe, M., Shiogama, H., Inoue, J., Kimoto, M., 2014. Robust Arctic sea-ice
690 influence on the frequent Eurasian cold winters in past decades. Nature Geoscience 7,
691 869-873.
692 Müller, J., Massé, G., Stein, R., Belt, S.T., 2009. Variability of sea-ice conditions in the Fram
693 Strait over the past 30,000 years. Nature Geoscience 2, 772-776.
694 Müller, J., Stein, R., 2014. High-resolution record of late glacial and deglacial sea ice
695 changes in Fram Strait corroborates ice–ocean interactions during abrupt climate
696 shifts. Earth and Planetary Science Letters 403, 446-455.
697 Müller, J., Wagner, A., Fahl, K., Stein, R., Prange, M., Lohmann, G., 2011. Towards
698 quantitative sea ice reconstructions in the northern North Atlantic: a combined
699 biomarker and numerical modelling approach. Earth and Planetary Science Letters
700 306, 137-148.

: “ Disclaimer: This is a pre-publication version. Readers are recommended to consult the full published version for accuracy and citation.”

Müller, J., Werner, K., Stein, R., Fahl, K., Moros, M., Jansen, E., 2012. Holocene cooling culminates in sea ice oscillations in Fram Strait. Quaternary Science Reviews 47, 1-14.

Navarro-Rodriguez, A. (2014) Reconstruction of Recent Palaeo Sea Ice Conditions in the Barents Sea. Ph.D. thesis, Plymouth University. URI: http://hdl.handle.net/10026.1/3085.

Navarro-Rodriguez, A., Belt, S.T., Knies, J., Brown, T.A., 2013. Mapping recent sea ice conditions in the Barents Sea using the proxy biomarker $IP_{25}$: implications for palaeo sea ice reconstructions. Quaternary Science Reviews 79, 26-39.

Overland, J.E., Wang, M., 2013. When will the summer Arctic be nearly sea ice free? Geophysical Research Letters 40, 2097-2101.

Oziel, L., Sirven, J., Gascard, J.C., 2016. The Barents Sea frontal zones and water masses variability (1980–2011). Ocean Science 12, 169-184.

Perovich, D.K., Polashenski, C., 2012. Albedo evolution of seasonal Arctic sea ice. Geophysical Research Letters 39, L08501. DOI: https://doi.org/10.1029/2012GL051432.

R Core Team, 2017. R: A language and environment for statistical computing. R Foundation for Statistical Computing, Vienna. <https://www.r-project.org>

Rampen, S.W., Abbas, B.A., Schouten, S., Sinninghe Damste, J.S., 2010. A comprehensive study of sterols in marine diatoms (Bacillariophyta): implications for their use as tracers for diatom productivity. Limnology and Oceanography 55, 91-105.

Rasmussen, T.L., Thomsen, E., 2015. Palaeoceanographic development in Storfjorden, Svalbard, during the deglaciation and Holocene: evidence from benthic foraminiferal records. Boreas 44, 24-44.

: “ Disclaimer: This is a pre-publication version. Readers are recommended to consult the full published version for accuracy and citation.”

Rasmussen, T.L., Thomsen, E., Ślubowska, M.A., Jessen, S., Solheim, A., Koç, N., 2007. Paleoceanographic evolution of the SW Svalbard margin (76°N) since 20,000 $^{14}$C yr BP. Quaternary Research 67, 100-114.

Ribeiro, S., Sejr, M.K., Limoges, A., Heikkilä, M., Andersen, T.J., Tallberg, P., Weckström, K., Husum, K., Forwick, M., Dalsgaard, T., Massé, G., Seidenkrantz, M.-S., Rysgaard, S., 2017. Sea ice and primary production proxies in surface sediments from a High Arctic Greenland fjord: Spatial distribution and implications for palaeoenvironmental studies. Ambio 46, 106-118.

Risebrobakken, B., Dokken, T., Smedsrud, L.H., Andersson, C., Jansen, E., Moros, M., Ivanova, E.V., 2011. Early Holocene temperature variability in the Nordic Seas: The role of oceanic heat advection versus changes in orbital forcing. Paleoceanography 26, PA4206. DOI: https://doi.org/10.1029/2011PA002117.

Risebrobakken, B., Moros, M., Ivanova, E.V., Chistyakova, N., Rosenberg, R., 2010. Climate and oceanographic variability in the SW Barents Sea during the Holocene. The Holocene 20, 609-621.

Rontani, J.-F., Belt, S.T., Amiraux, R., 2018a. Biotic and abiotic degradation of the sea ice diatom biomarker $IP_{25}$ and selected algal sterols in near-surface Arctic sediments. Organic Geochemistry 118, 73-88.

Rontani, J.-F., Belt, S.T., Brown, T.A., Vaultier, F., Mundy, C.J., 2014a. Sequential photo- and autoxidation of diatom lipids in Arctic sea ice. Organic Geochemistry 77, 59-71.

Rontani, J.F., Aubert, C., Belt, S.T., 2018b. Electron ionization mass spectrometry fragmentation and multiple reaction monitoring quantification of bacterial metabolites of the sea ice biomarker proxy $IP_{25}$ in Arctic sediments. Rapid Communications in Mass Spectrometry 32, 775-783.

: " Disclaimer: This is a pre-publication version. Readers are recommended to consult the full published version for accuracy and citation."

749 Rontani, J.F., Belt, S.T., Vaultier, F., Brown, T.A., Massé, G., 2014b. Autoxidative and
750 photooxidative reactivity of highly branched isoprenoid (HBI) alkenes. Lipids 49,
751 481-494.
752 Rowland, S.J., Allard, W.G., Belt, S.T., Massé, G., Robert, J.M., Blackburn, S., Frampton,
753 D., Revill, A.T., Volkman, J.K., 2001. Factors influencing the distributions of
754 polyunsaturated terpenoids in the diatom, *Rhizosolenia setigera*. Phytochemistry 58,
755 717-728.
756 Ruan, J., Huang, Y., Shi, X., Liu, Y., Xiao, W., Xu, Y., 2017. Holocene variability in sea
757 surface temperature and sea ice extent in the northern Bering Sea: a multiple
758 biomarker study. Organic Geochemistry 113, 1-9.
759 Rüther, D.C., Bjarnadóttir, L.R., Junttila, J., Husum, K., Rasmussen, T.L., Lucchi, R.G.,
760 Andreassen, K., 2012. Pattern and timing of the northwestern Barents Sea Ice Sheet
761 deglaciation and indications of episodic Holocene deposition. Boreas 41, 494-512.
762 Sakshaug, E., Johnsen, G.H., Kovacs, K.M., 2009. Ecosystem Barents Sea. Tapir Academic
763 Press, Trondheim, Norway. ISBN: 9788251924610.
764 Screen, J.A., Simmonds, I., 2010. The central role of diminishing sea ice in recent Arctic
765 temperature amplification. Nature 464, 1334-1337.
766 Serreze, M.C., Barry, R.G., 2011. Processes and impacts of Arctic amplification: a research
767 synthesis. Global and Planetary Change 77, 85-96.
768 Ślubowska, M.A., Koç, N., Rasmussen, T.L., Klitgaard-Kristensen, D., 2005. Changes in the
769 flow of Atlantic water into the Arctic Ocean since the last deglaciation: Evidence
770 from the northern Svalbard continental margin, 80°N. Paleoceanography 20, PA4014.
771 DOI: https://doi.org/10.1029/2005PA001141.
772 Smedsrud, L.H., Esau, I., Ingvaldsen, R.B., Eldevik, T., Haugan, P.M., Li, C., Lien, V.S.,
773 Olsen, A., Omar, A.M., Otterå, O.H., Risebrobakken, B., Sandø, A.B., Semenov,

: " Disclaimer: This is a pre-publication version. Readers are recommended to consult the full published version for accuracy and citation."

V.A., Sorokina, S.A., 2013. The role of the Barents Sea in the Arctic climate system. Reviews of Geophysics 51, 415-449.

Smedsrud, L.H., Ingvaldsen, R., Nilsen, J.E.Ø., Skagseth, Ø., 2010. Heat in the Barents Sea: transport, storage, and surface fluxes. Ocean Science 6, 219-234.

Smik, L., Cabedo-Sanz, P., Belt, S.T., 2016. Semi-quantitative estimates of paleo Arctic sea ice concentration based on source-specific highly branched isoprenoid alkenes: a further development of the $PIP_{25}$ index. Organic Geochemistry 92, 63-69.

Sorteberg, A., Kvingedal, B., 2006. Atmospheric forcing on the Barents Sea winter ice extent. Journal of Climate 19, 4772-4784.

Stein, R., Fahl, K., 2012. A first southern Lomonosov Ridge (Arctic Ocean) 60 ka $IP_{25}$ sea-ice record. Polarforschung, 83-86.

Stein, R., Fahl, K., 2013. Biomarker proxy shows potential for studying the entire Quaternary Arctic sea ice history. Organic Geochemistry 55, 98-102.

Stein, R., Fahl, K., Schreck, M., Knorr, G., Niessen, F., Forwick, M., Gebhardt, C., Jensen, L., Kaminski, M., Kopf, A., Matthiessen, J., Jokat, W., Lohmann, G., 2016. Evidence for ice-free summers in the late Miocene central Arctic Ocean. Nature Communications 7, 11148. DOI: https://doi.org/10.1038/ncomms11148.

Stoynova, V., Shanahan, T.M., Hughen, K.A., de Vernal, A., 2013. Insights into Circum-Arctic sea ice variability from molecular geochemistry. Quaternary Science Reviews 79, 63-73.

Stroeve, J.C., Blanchard-Wrigglesworth, E., Guemas, V., Howell, S., Massonnet, F., Tietsche, S., 2015. Improving predictions of Arctic sea ice extent. Eos 96. DOI: https://doi.org/10.1029/2015EO031431.

Vancoppenolle, M., Meiners, K.M., Michel, C., Bopp, L., Brabant, F., Carnat, G., Delille, B., Lannuzel, D., Madec, G., Moreau, S., Tison, J.-L., van der Merwe, P., 2013. Role of

: “ Disclaimer: This is a pre-publication version. Readers are recommended to consult the full published version for accuracy and citation.”

799 sea ice in global biogeochemical cycles: emerging views and challenges. Quaternary
800 Science Reviews 79, 207-230.
801 Vare, L.L., Massé, G., Belt, S.T., 2010. A biomarker-based reconstruction of sea ice
802 conditions for the Barents Sea in recent centuries. The Holocene 20, 637-643.
803 Vihma, T., 2014. Effects of Arctic sea ice decline on weather and climate: a review. Surveys
804 in Geophysics 35, 1175-1214.
805 Vinje, T., 2001. Anomalies and trends of sea-ice extent and atmospheric circulation in the
806 Nordic Seas during the period 1864–1998. Journal of Climate 14, 255-267.
807 Volkman, J.K., 1986. A review of sterol markers for marine and terrigenous organic matter.
808 Organic Geochemistry 9, 83-99.
809 Volkman, J.K., 2006. Lipid markers for marine organic matter, In: Volkman, J.K. (Ed.),
810 Marine organic matter: biomarkers, isotopes and DNA. Springer Berlin Heidelberg,
811 Berlin, Heidelberg, pp. 27-70.
812 Walsh, J.E., Fetterer, F., Scott Stewart, J., Chapman, W.L., 2017. A database for depicting
813 Arctic sea ice variations back to 1850. Geographical Review 107, 89-107.
814 Wassmann, P., Ratkova, T., Andreassen, I., Vernet, M., Pedersen, G., Rey, F., 1999. Spring
815 bloom development in the marginal ice zone and the central Barents Sea. Marine
816 Ecology 20, 321-346.
817 Wassmann, P., Reigstad, M., Haug, T., Rudels, B., Carroll, M.L., Hop, H., Gabrielsen, G.W.,
818 Falk-Petersen, S., Denisenko, S.G., Arashkevich, E., Slagstad, D., Pavlova, O., 2006.
819 Food webs and carbon flux in the Barents Sea. Progress in Oceanography 71, 232-
820 287.
821 Weckström, K., Massé, G., Collins, L.G., Hanhijärvi, S., Bouloubassi, I., Sicre, M.-A.,
822 Seidenkrantz, M.-S., Schmidt, S., Andersen, T.J., Andersen, M.L., Hill, B., Kuijpers,

: " Disclaimer: This is a pre-publication version. Readers are recommended to consult the full published version for accuracy and citation."

A., 2013. Evaluation of the sea ice proxy $IP_{25}$ against observational and diatom proxy data in the SW Labrador Sea. Quaternary Science Reviews 79, 53-62.

Werner, K., Müller, J., Husum, K., Spielhagen, R.F., Kandiano, E.S., Polyak, L., 2016. Holocene sea subsurface and surface water masses in the Fram Strait – Comparisons of temperature and sea-ice reconstructions. Quaternary Science Reviews 147, 194-209.

Werner, K., Spielhagen, R.F., Bauch, D., Hass, H.C., Kandiano, E., 2013. Atlantic Water advection versus sea-ice advances in the eastern Fram Strait during the last 9 ka: multiproxy evidence for a two-phase Holocene. Paleoceanography 28, 283-295.

Xiao, X., Fahl, K., Müller, J., Stein, R., 2015a. Sea-ice distribution in the modern Arctic Ocean: Biomarker records from trans-Arctic Ocean surface sediments. Geochimica et Cosmochimica Acta 155, 16-29.

Xiao, X., Fahl, K., Stein, R., 2013. Biomarker distributions in surface sediments from the Kara and Laptev seas (Arctic Ocean): indicators for organic-carbon sources and sea-ice coverage. Quaternary Science Reviews 79, 40-52.

Xiao, X., Stein, R., Fahl, K., 2015b. MIS 3 to MIS 1 temporal and LGM spatial variability in Arctic Ocean sea ice cover: reconstruction from biomarkers. Paleoceanography 30, 969-983.

Yunker, M.B., Belicka, L.L., Harvey, H.R., Macdonald, R.W., 2005. Tracing the inputs and fate of marine and terrigenous organic matter in Arctic Ocean sediments: a multivariate analysis of lipid biomarkers. Deep Sea Research Part II: Topical Studies in Oceanography 52, 3478-3508.

## Figure Legends

: " Disclaimer: This is a pre-publication version. Readers are recommended to consult the full published version for accuracy and citation."

847 **Figure 1.** Structures of $C_{25}$ Highly-Branched Isoprenoid (HBI) biomarkers used for sea ice
848 reconstruction in the current study.

849 **Figure 2.** Map of the Barents Sea showing locations of downcore records 1200, 11, and 70
850 (labelled black squares). The maximum April–June sea ice edge for the 1988–2007 period
851 corresponding to an SpSIC threshold of 0 % is shown by a solid black line. Circles
852 correspond to surface sediments used for CT model training, with overlying marginal (<10%
853 satellite SpSIC; red markers), intermediate (10–50% SpSIC; yellow markers), and extensive
854 (>50% SpSIC; green markers) sea ice cover. A simplified representation of the major AW
855 surface currents is illustrated by red arrows, with abbreviations for: WSC – West Spitsbergen
856 Current; NCaC – North Cape Current.

857 **Figure 3.** Proxy data and correlations for core 70 (northern Barents Sea): (a) Absolute
858 concentrations of $IP_{25}$ (black line with circle markers) and HBI III (Z; green line); (b) $P_{III}IP_{25}$-
859 based % SpSIC profile (black line) with an RMSE error of ca. 11% (thin black lines; Smik et
860 al., 2016; Köseoğlu et al., 2018) and superimposed CT predictions of marginal (red circles),
861 intermediate (yellow squares), and extensive (green diamonds) sea ice cover. Dashed
862 horizontal lines represent the satellite SpSIC boundaries used to separate the sea ice classes in
863 the CT model (Köseoğlu et al., 2018), where 10% and 50% satellite SpSIC thresholds
864 correspond to the marginal-intermediate and intermediate-extensive boundaries, respectively;
865 (c) Running Pearson's correlations for $IP_{25}$ versus HBI II (black line with circle markers) and
866 HBI III (Z) versus HBI III (E; red line) with a sampling window of 9 core horizons. Grey
867 diamonds represent correlations significant at $p = 0.05$, and the dashed line separates positive
868 ($r > 0$) and negative ($r < 0$) correlations.

: " Disclaimer: This is a pre-publication version. Readers are recommended to consult the full published version for accuracy and citation."

869 **Figure 4.** Proxy data and correlations for core 1200 (southwestern Barents Sea). The
870 illustrated profiles are analogous to those shown in Fig. 3. The light blue vertical bar
871 highlights the Younger Dryas stadial (12.95–11.70 cal kyr BP).

872 **Figure 5.** Proxy data and correlations for core 11 (western Barents Sea). The illustrated
873 profiles are analogous to those shown in Figs. 3 and 4. In (b), crossed red squares represent
874 horizons where the discrepancy between CT predictions and $P_{III}IP_{25}$-based SpSIC estimates
875 exceeded the $P_{III}IP_{25}$–SpSIC calibration RMSE of ca. 11% (Smik et al., 2016). The light blue
876 vertical bar highlights the Younger Dryas stadial (12.95–11.70 cal kyr BP).

877 **Figure 6**. Biomarker profiles and correlations for core 11: (a) Concentrations of $IP_{25}$ and HBI
878 II represented by black (with circle markers) and green lines, respectively; (b) Running
879 correlation of first relative (%) differences, with a sampling window of 9 horizons. Positive
880 and negative correlations are separated by a dashed horizontal line, while grey diamonds
881 show correlations significant at a 95% confidence level. In both (a) and (b), crossed red
882 squares represent samples for which CT model predictions significantly differed from
883 $P_{III}IP_{25}$-derived % SpSIC values, with a discrepancy exceeding the RMSE of the $P_{III}IP_{25}$–
884 SpSIC calibration (ca. ±11% SpSIC). The light blue vertical bar highlights the Younger
885 Dryas stadial (12.95–11.70 cal kyr BP).

886 **Figure 7**. Pearson's correlations of $IP_{25}$ versus HBI II (upper panel series A) and HBI III (Z)
887 versus HBI III (E) (lower panel series B) in Barents Sea surface sediments with marginal
888 (<10% SpSIC; red circles), intermediate (10–50% SpSIC; yellow triangles), and extensive
889 (>50% SpSIC; green squares) overlying sea ice conditions. Surface sediment biomarker data
890 was taken from Köseoğlu et al. (2018).

891 **Figure 8**. Biomarker composition and CT model output for cores 70, 1200, and 11 using
892 different RF combinations: (a) Averaged relative abundances of $IP_{25}$ and HBIs II, III (Z) and

: “ Disclaimer: This is a pre-publication version. Readers are recommended to consult the full published version for accuracy and citation.”

III (E) in surface sediments and cores using calibrated and arbitrarily equated (uncalibrated) RFs; (b) Percentage distribution of core horizons classified into three categories of sea ice conditions by the CT model. “Correct RFs” and “incorrect RFs” indicate the respective use of calibrated RFs and arbitrarily equated RFs for both the CT training set (surface sediments) and cores. “Mismatched RFs” represents the use of calibrated and uncalibrated RFs for the training set and downcore records, respectively. Values within white circles correspond to the number of horizons classified into a given category of sea ice conditions where a discrepancy with $P_{III}IP_{25}$-based SpSIC estimates of at least 1% was observed. No samples were misclassified into the extensive (>50% SpSIC) sea ice category.

: “ Disclaimer: This is a pre-publication version. Readers are recommended to consult the full published version for accuracy and citation.”

**Figure 1**

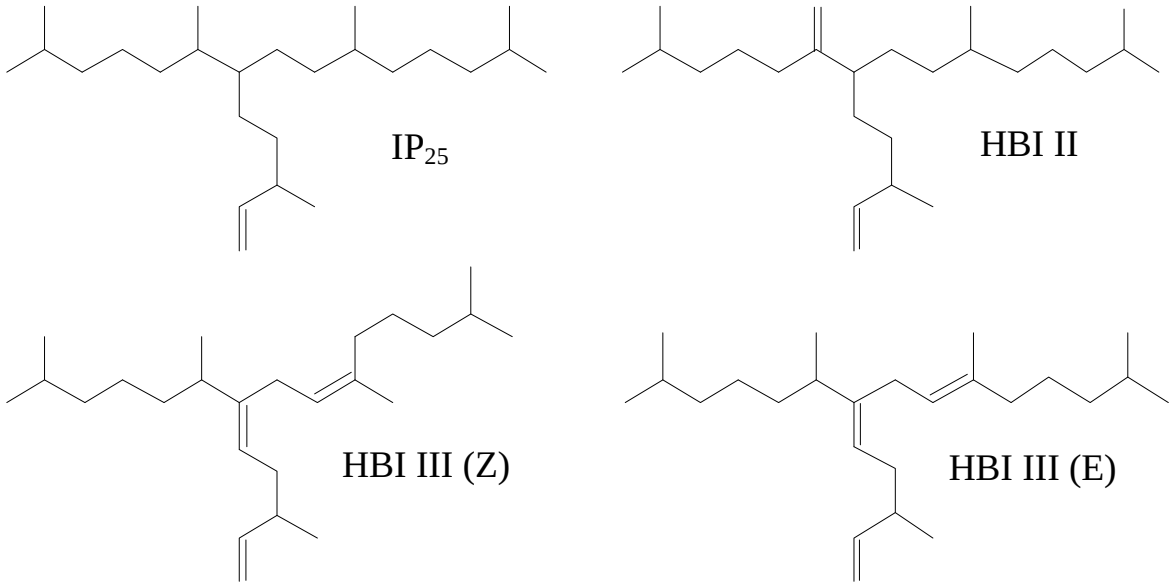

**Figure 2**

: “ Disclaimer: This is a pre-publication version. Readers are recommended to consult the full published version for accuracy and citation.”

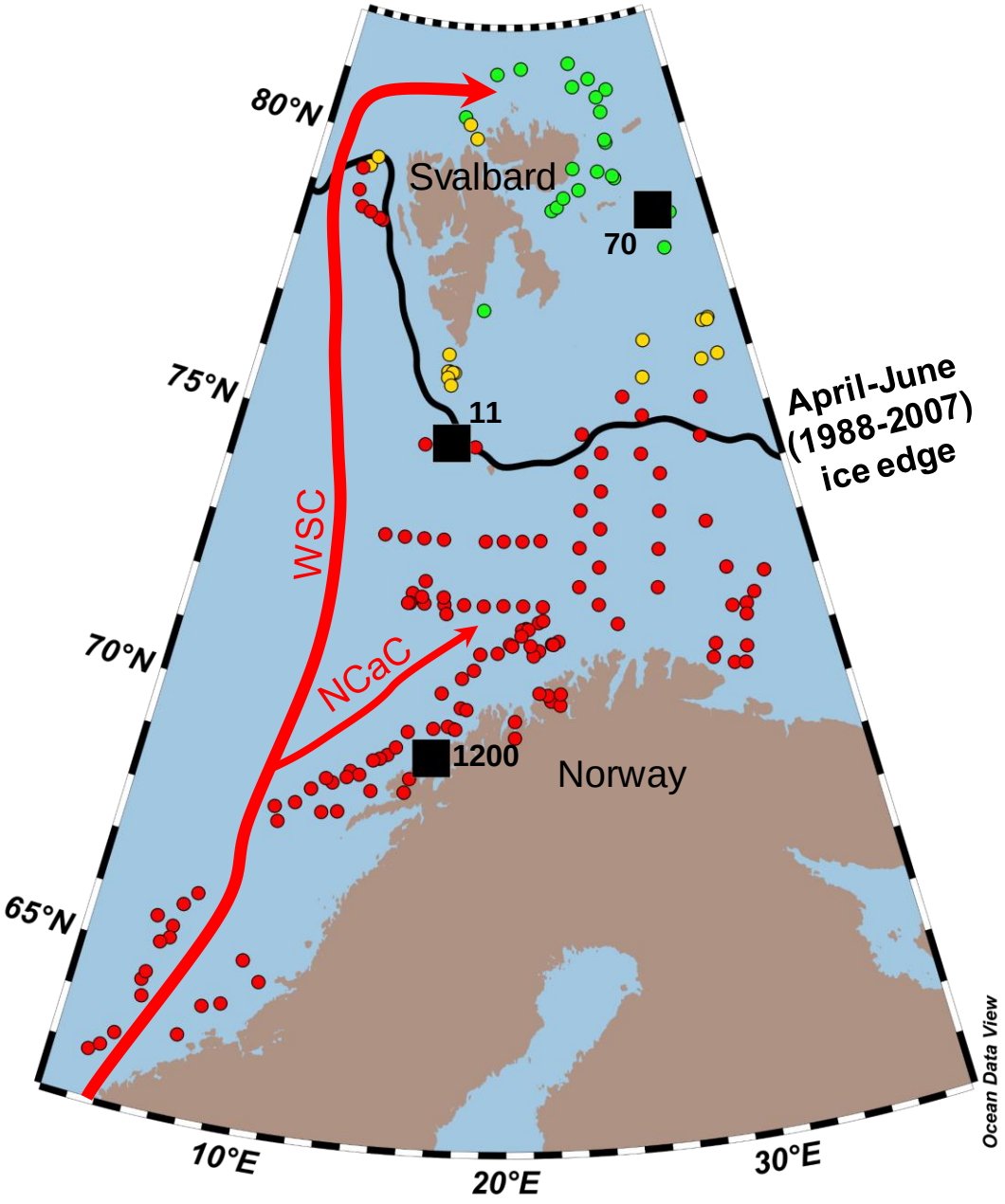

**Figure 3**

: " Disclaimer: This is a pre-publication version. Readers are recommended to consult the full published version for accuracy and citation."

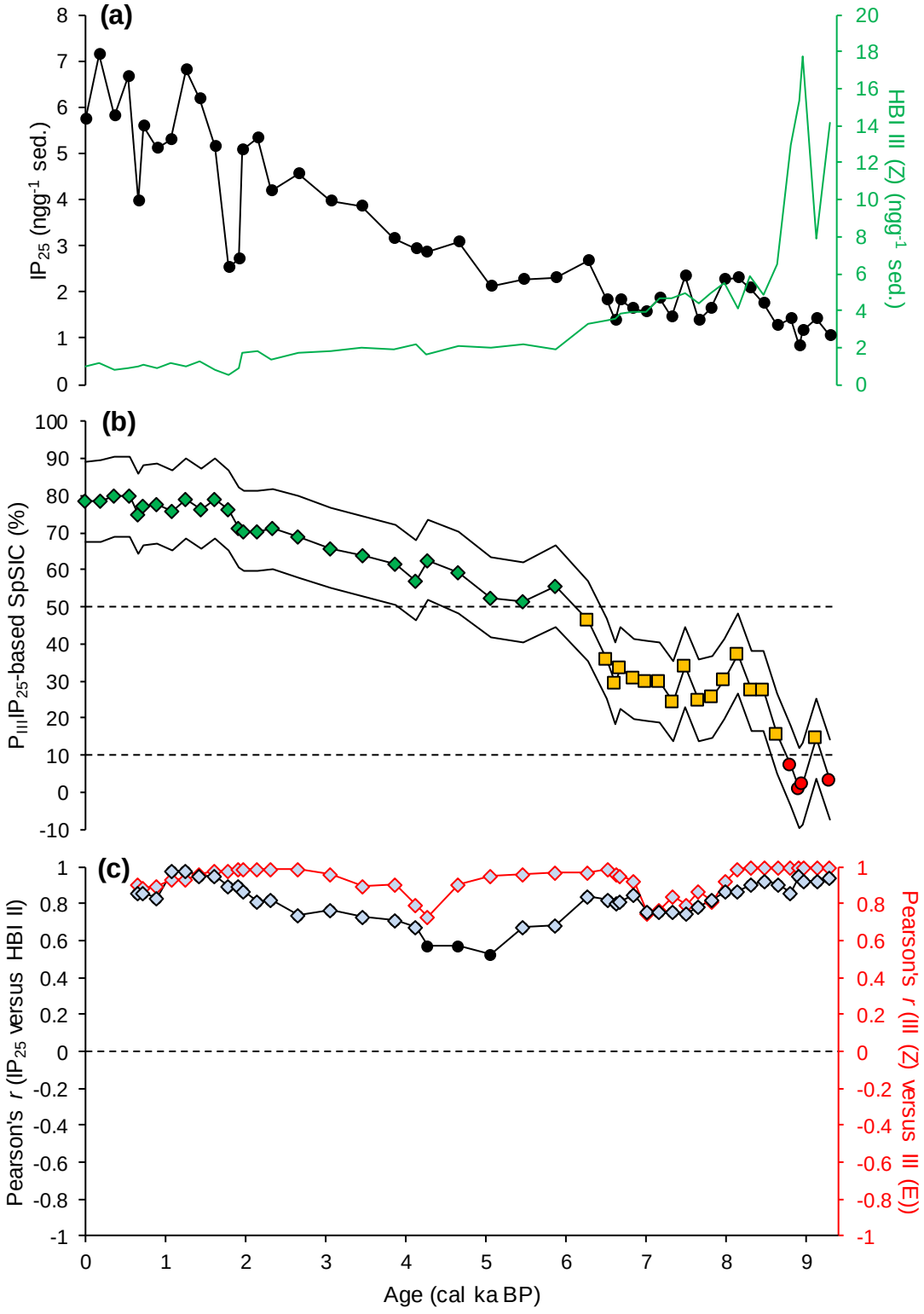

**Figure 4**

: " Disclaimer: This is a pre-publication version. Readers are recommended to consult the full published version for accuracy and citation."

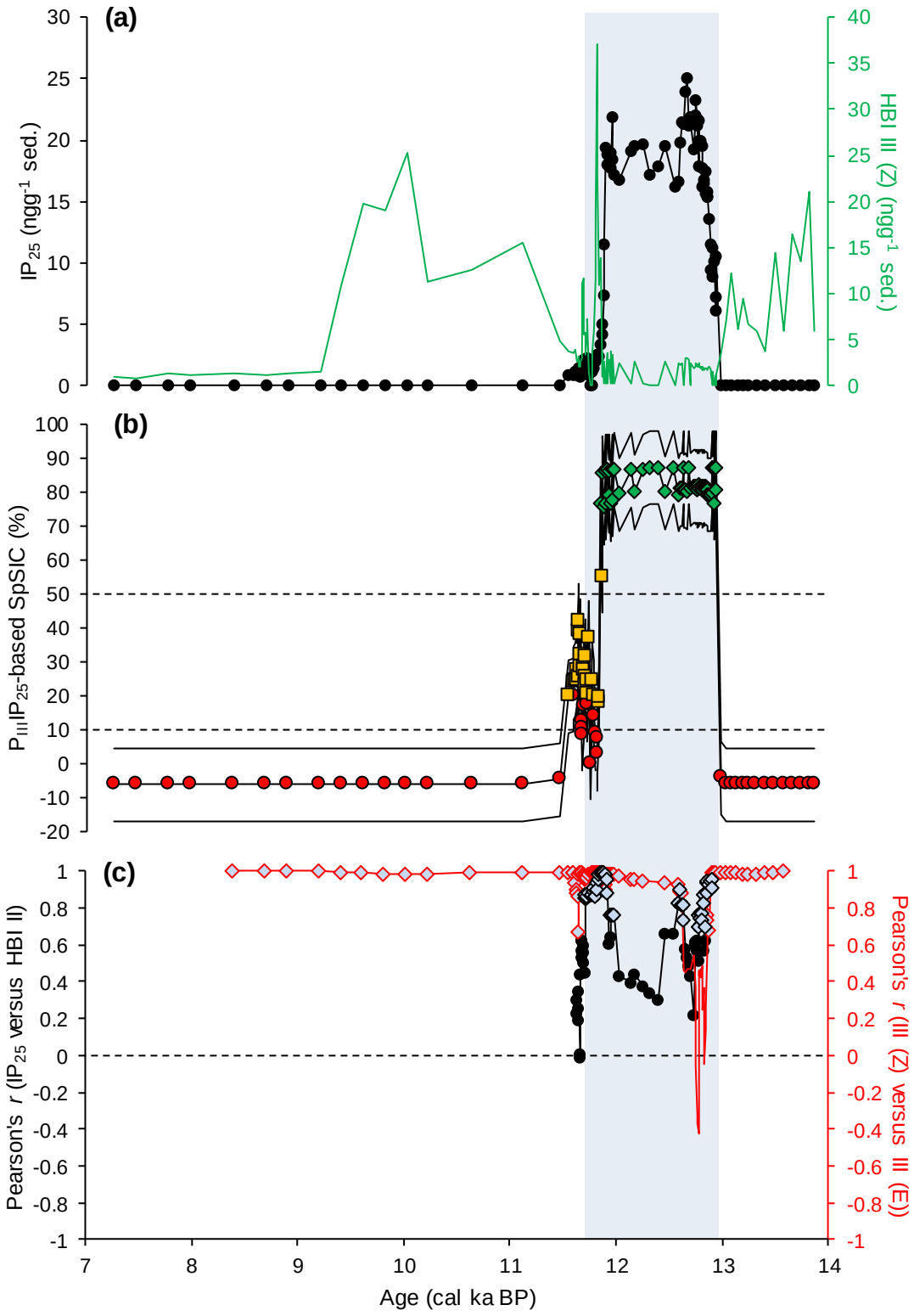

**Figure 5**

: " Disclaimer: This is a pre-publication version. Readers are recommended to consult the full published version for accuracy and citation."

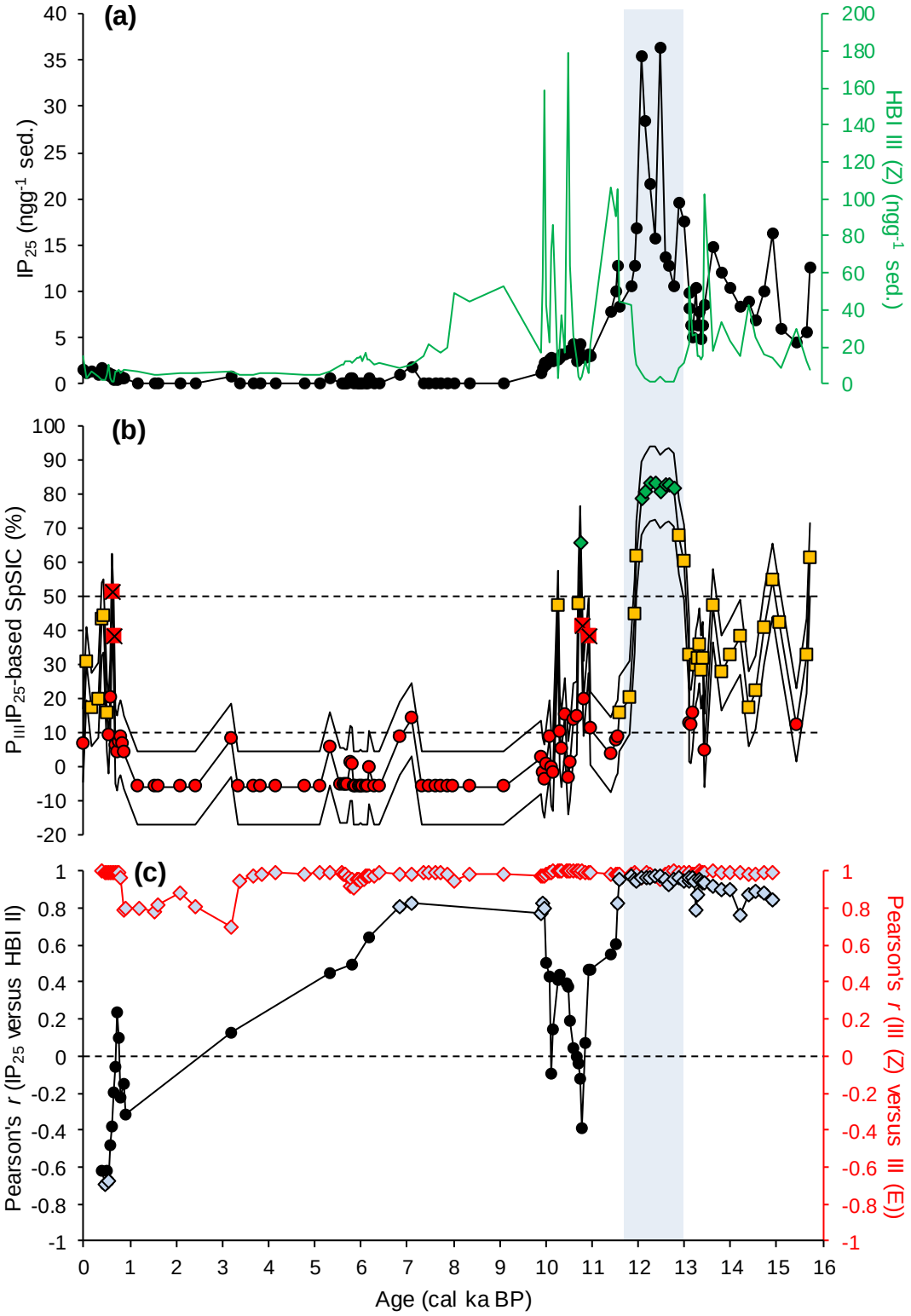

**Figure 6**

: " Disclaimer: This is a pre-publication version. Readers are recommended to consult the full published version for accuracy and citation."

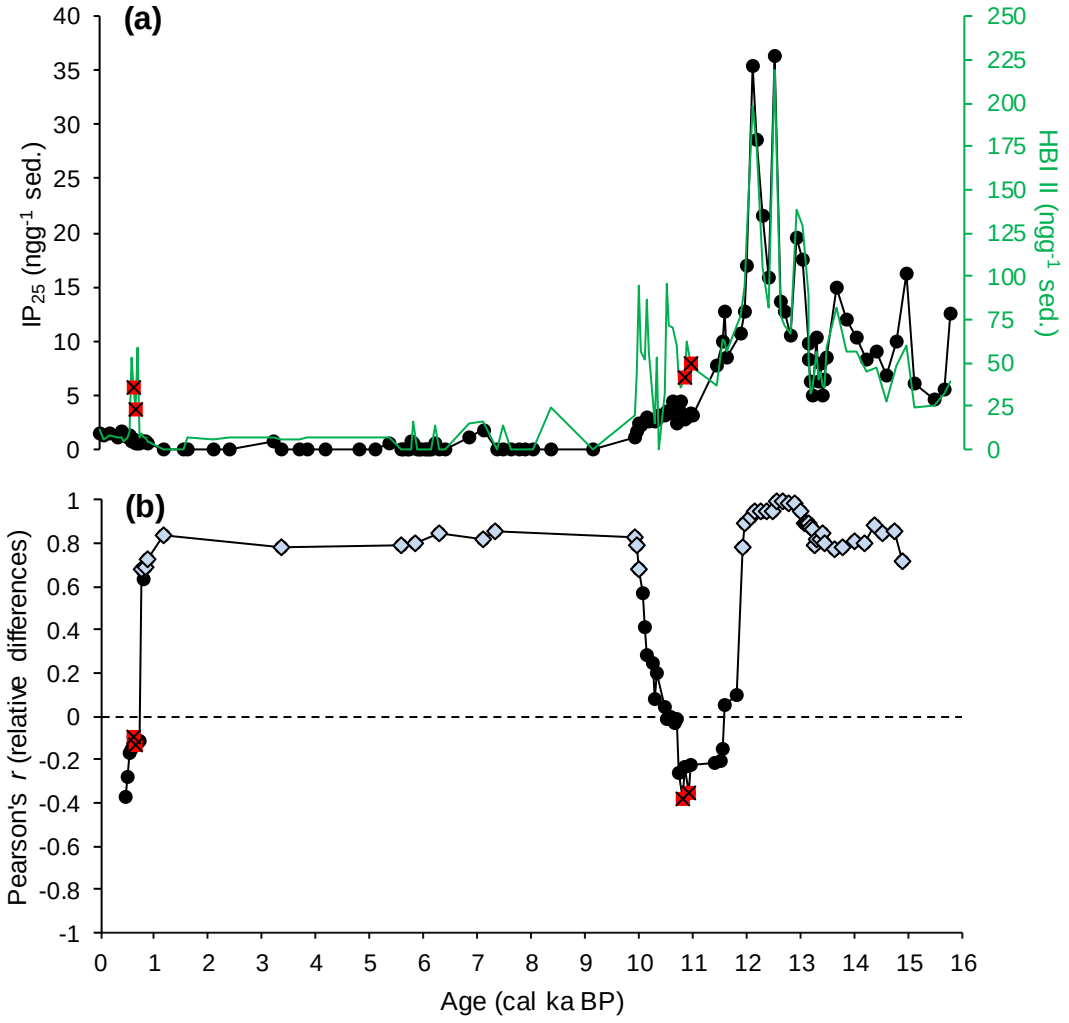

: “ Disclaimer: This is a pre-publication version. Readers are recommended to consult the full published version for accuracy and citation.”

## Figure 7

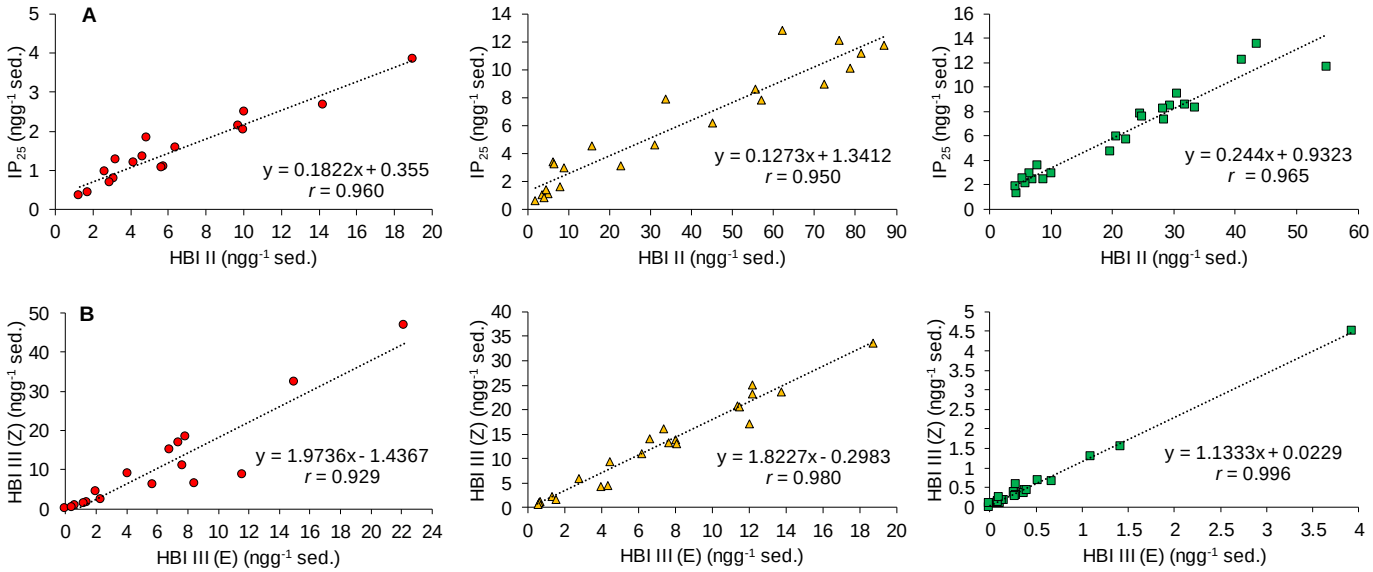

: “ Disclaimer: This is a pre-publication version. Readers are recommended to consult the full published version for accuracy and citation.”

**Figure 8**